Journal of Thermal Analysis and Calorimetry (2021) 143:523–533
https://doi.org/10.1007/s10973-019-09253-x

Improving the efficiency of an exhaust thermoelectric generator based on changes in the baffle distribution of the heat exchanger

Roozbeh Sheikh[1] · Seifollah Gholampour[2] · Hossein Fallahsohi[3] · Marjan Goodarzi[4] · Majid Mohammad Taheri[2] · Mehdi Bagheri[5]

Received: 11 October 2019 / Accepted: 29 December 2019 / Published online: 9 January 2020

Abstract

A significant amount of the heat is lost in the vehicle exhaust and simply transferred to the environment. Using a thermoelectric generator (TEG), it is becoming possible to convert this heat potential into the electrical energy. In this study, nine types of the heat exchangers in three different groups, namely A, B, and C are modeled in three dimensions and studied using computational fluid dynamics (CFD) analysis with various baffle arrangements to obtain electrical energy from the vehicle exhaust. The modeling of the group A is focused on the effect of the angle and thickness of the baffles at the inlet of the heat exchanger. In the group B, the distances between the baffles and their heights are changed, and group C is focused to model larger baffles with different arrangements. The results show that, the pressure drop is in the permissible range in all the models, and the gas flow velocity in group A is almost similar to what studied in other models; however, the power produced in it is at least 7.25% higher than other models. The best model for the highest generated power is also recommended and discussed. It is also shown that implementation of a deflector will lead to a non-uniform and unidirectional distribution of temperature. The results also reveal that under identical conditions in the middle section of the heat exchanger, reducing the height of the baffles from 8.46 mm to 2.30 mm will result 10.88% decrease in the output power. Furthermore, increasing the distance between the baffles from 5.2 mm to 16.8 mm will cause 3.91% increase in the output power.

Keywords Thermoelectric generators · Heat exchanger · Baffles · Temperature distribution · Power · Pressure drop

Introduction

Nowadays, one of the major concerns in the world is the global warming and its harmful impact over the environment. Given the international concerns for reducing greenhouse gas production and increasing the efficiency of thermal systems to prevent energy dissipation, different studies and research methods on energy recovery in thermal systems have been conducted and elaborated in the recent years [1–4]. The heat waste recovery method is the recovery of the thermal energy lost in vehicles exhaust using thermoelectric generators (TEGs), which convert the temperature difference between a cold and a hot panel to electrical energy based on the Seebeck effect [5, 6]. TEGs consist of several n-type and p-type semiconductors, and the

✉ Seifollah Gholampour
s.gholampour@iau-tnb.ac.ir

Roozbeh Sheikh
roozbeh.sheikh@srbiau.ac.ir

Hossein Fallahsohi
hossein.fallahsohi@gmail.com

Marjan Goodarzi
marjan.goodarzi@tdtu.edu.vn

Majid Mohammad Taheri
majid.mohamadtaheri@gmail.com

Mehdi Bagheri
mehdi.bagheri@nu.edu.kz

1 Department of Mathematics, Science and Research Branch, Islamic Azad University, Tehran, Iran

2 North Tehran Branch, Faculty of Electrical and Computer Engineering, Islamic Azad University, P.O.B. 1651153311, Tehran, Iran

3 Department of Energy Systems, North Tehran Branch, Islamic Azad University, Tehran, Iran

4 Sustainable Management of Natural Resources and Environment Research Group, Faculty of Environment and Labour Safety, Ton Duc Thang University, Ho Chi Minh City, Vietnam

5 Department of Electrical and Computer Engineering, School of Engineering and Digital Sciences, Nazarbayev University, Nur-Sultan, Kazakhstan

most important factors affecting the ZT include the material, the coefficient of thermal conductivity and electrical conductivity [7, 8]. The effectiveness of using TEGs on the exhaust and heat exchanger of vehicles have been studied in the literatures [9–11]. The heat exchangers are used for the evaluation of optimum temperature distribution to obtain more electrical power produced by the TEG in [12–14]. Furthermore, some papers demonstrate that to produce more electrical power, it is possible to make the temperature distribution more uniform over the surface of the heat exchanger, [15, 16]. Niu et al investigate the effect of baffle angle over heat transfer to TEGs [17]. In [18] it is demonstrated and discussed that employing many small fins leads to a uniform temperature distribution in the heat exchanger. In [19, 20], a computational fluid dynamics (CFD) analysis is performed to study the impact of material and surface area on the temperature distribution in the heat exchanger. Moreover, adding a cooling source to the TEGs for increasing efficiency is studied by [21]. Liu et al explored the relationship between engine revolution and TEG output power by comparing the effect of the former [22]. They also studied the impact of placing the heat exchanger after the catalytic converter and before the muffler on optimizing the temperature distribution [23]. Some researchers studied the geometries of fins and folded plates and their effects on temperature distribution and pressure drop [24–29]. Liu et al studied acoustic attenuation behavior in [30]. By creating dimples on the surface of the heat exchanger in other research, they calculated the drop in the pressure loss [31, 32]. Some literatures obtained a more satisfactory temperature distribution by implementing a cylinder structure along with some fins inside the heat exchanger [33, 34]. Lu et al evaluated the temperature variations and shown the changes in the output power by considering a different winglet configuration [35]. Through CFD analysis and mathematical modeling, Wang et al studied the temperature distribution and the output power using inserted fins and a dimpled surface in the heat exchanger and studied the effects of the pressure drop and power factor over the performance of the TEG [36].

Previous researches have confirmed the high impact of baffles arrangement in the efficiency of an exhaust TEG. Hence, this research study provides a more optimal strategy for the structure and distribution of small baffles. Each baffle is designed with specific deviation degrees and dimensions. These baffles have been designed to achieve a more uniform and more optimal temperature distribution and uniform distribution of temperature. It has also paid attention to calculate the pressure drop and gas velocity during this optimization so while the maximum usage that each TEG module can obtain from the distributed temperature, there is no damage to the vehicle engines. By providing special strategies for baffles and the facility to increase the gas temperature, it has been attempted to obtain maximum electrical power using TEG.

Materials and methods

Design of study

In this research, an arrangement strategy with identical outer dimensions was considered and modeled using SOLIDWORKS 2017, as shown in Fig. 1, for designing the internal space of the 9 heat exchangers. Each of these models consists front, middle, and rear sections. The middle section is in the shape of a rectangular cuboid and has dimensions $390 \times 310 \times 22$ mm. The diameter of the inlet and outlet sections of the heat exchanger has been considered to be 36 mm. As shown in Fig. 1c, the heat exchangers in the model A strategy is different in terms of dimension type, size, and baffle angles at the inlet. In model B's strategy, the baffle arrangements in the middle section of the heat exchanger are different in terms of distances between baffles (Fig. 1d). Moreover, the model C's strategy focuses on non-perpendicular baffle angles in a chaos-shaped arrangement (Fig. 1e). In models A_1 and A_2, two baffle angles were 50° and 40° in the front section, and the thickness of the baffles has been assumed to be 5 mm. However, in model A_3, the baffle angle and inlet thickness have been taken as 50° and 10 mm, respectively. Also, the placement distances of the baffles concerning the inlet of the heat exchanger have been changed. In all three models A_1, A_2, and A_3, six rows of discontinuous baffles have been installed in the middle section with a distance of 5.2 mm between neighboring baffles. The height of each baffle has been considered to be 8.46 mm. The distances between the baffles in the six rows of models B_1 and B_2 have been defined as 5.2 mm and 16.8 mm, respectively (Fig. 1d). Unlike models A_1, A_2, and A_3, the baffles heights are considered to be 2.3 mm in models B_1 and B_2. In model B_3, the authors have tried to re-evaluate the model by eliminating 2 baffles in the front section and adding 2 deflectors in the middle section of the heat exchanger. In model C_1, the baffles in the middle section are not connected to the top and bottom surfaces of the heat exchanger. Also, the arrangement and type of baffles have changed in models C_1 and C_2, as shown in Fig. 1e. It should be noted that the 9 models presented have been gradually completed and studied on a step-by-step basis by analyzing the results of the initial models.

Formulation

There were various developments in the optimization of thermal equations for accurate calculation of thermal distribution [36, 37]. The thermal-CFD analysis method was used to evaluate the temperature distribution. Similar to previous research, it has been assumed in this simulation that the inlet of the heat exchanger is connected to the catalytic

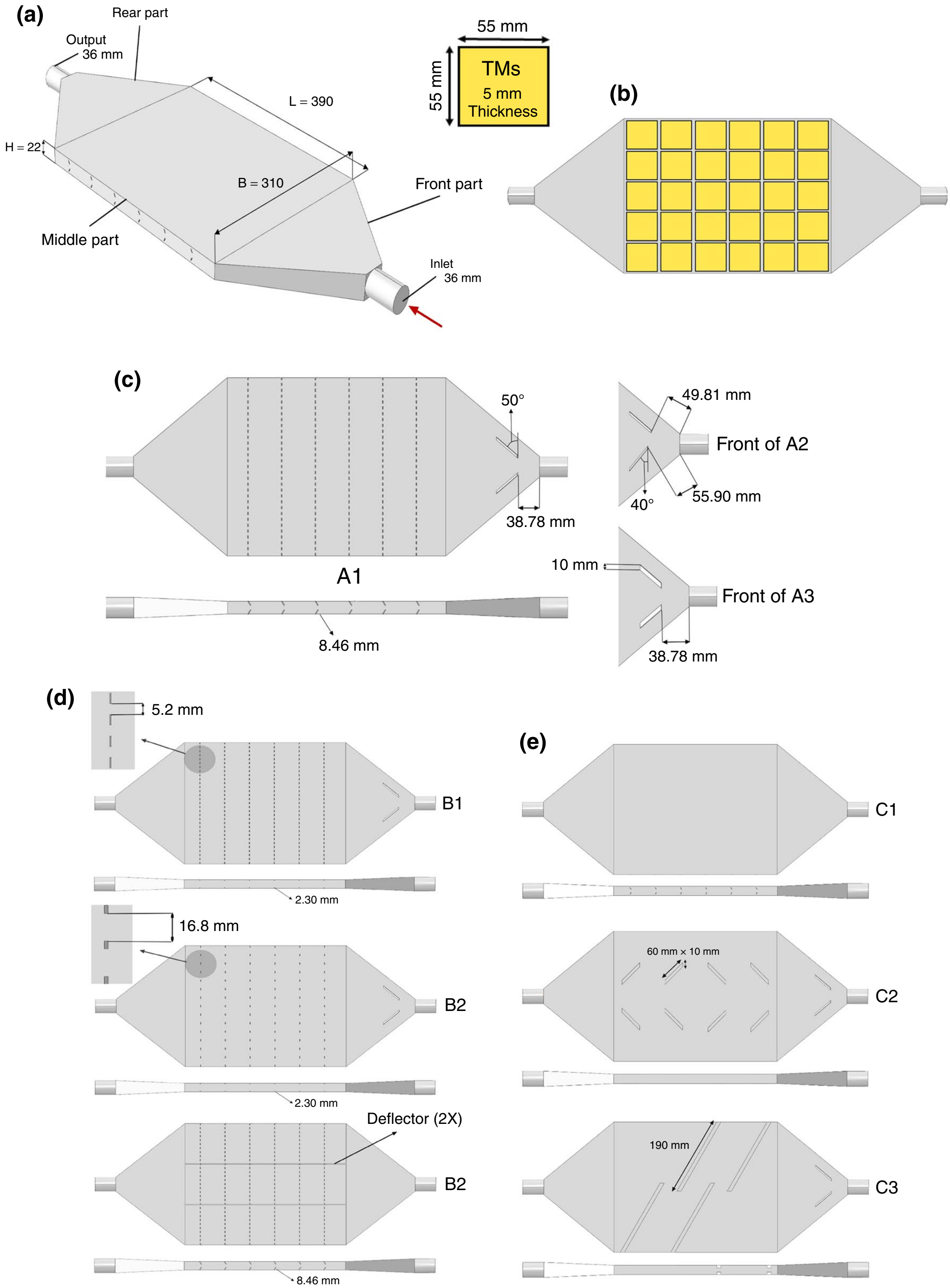

Fig. 1 **a** Dimensions and external surfaces of the heat exchanger, **b** arrangement of thermoelectric modules, **c** baffle arrangement in the internal structure of the heat exchanger in group A, **d** and **e** baffle arrangement in groups B and C

converter, and its outlet is connected to the muffler. Also, 60 thermoelectric modules have been placed on the top and bottom surfaces of the heat exchanger [21, 32]. The dimensions of each thermoelectric module are 55 mm × 55 mm × 5 mm (Fig. 1b). In this research, the gas flow is considered to be steady state and incompressible, and the K–ε turbulence model adopted to compute heat transfer and flow field has been used to predict the flow, as described by Eqs. 1–7 [24, 38–40].

Turbulent kinetic energy equation:

$$\frac{\partial(\rho u_i k)}{\partial x_i} = \frac{\partial}{\partial x_i}\left[\left(\mu + \frac{\mu_t}{\sigma_k}\right)\frac{\partial k}{\partial x_i}\right] + P_k - \rho\varepsilon, \tag{1}$$

Turbulent energy dissipation rate equation:

$$\frac{\partial(\rho u_i \varepsilon)}{\partial x_i} = \frac{\partial}{\partial x_i}\left[\left(\mu + \frac{\mu_t}{\sigma_\varepsilon}\right)\frac{\partial \varepsilon}{\partial x_i}\right] + \frac{\varepsilon}{k}\left(C_{\varepsilon 1}P_k - C_{\varepsilon 2}\rho\varepsilon\right), \tag{2}$$

Turbulent viscosity:

$$\mu_t = C_\mu \rho \frac{k^2}{\varepsilon}, \tag{3}$$

Continuity equation:

$$\frac{\partial(\rho u_i)}{\partial x_i} = 0, \tag{4}$$

Momentum equation:

$$\frac{\partial(\rho u_i u_j)}{\partial x_i} = \frac{\partial}{\partial x_i}\left(\mu\frac{\partial u_j}{\partial x_j}\right) - \frac{\partial p}{\partial x_j}, \tag{5}$$

Energy equation:

$$\frac{\partial(\rho u_i t)}{\partial x_i} = \frac{\partial}{\partial x_i}\left(\frac{k}{C_p}\frac{\partial t}{\partial x_i}\right), \tag{6}$$

Empirical constants:

$$C_{\varepsilon 1} = 1.44,\ C_{\varepsilon 2} = 1.92,\ C_\mu = 0.09,\ \sigma_k = 1,\ \sigma_\varepsilon = 1.3\ [25] \tag{7}$$

where ρ is the density of exhaust gas, u_i (i = 1,2,3) and u_j (j = 1,2,3) are the velocity components, x_i (i = 1,2,3) and x_j (j = 1,2,3) are rectangular coordinates, μ is the kinetic viscosity, μ_t is the turbulent eddy viscosity, k is the turbulence kinetic energy, ε is the turbulence energy dissipation rate, and P_k is the shear production of turbulent kinetic energy [23].

As similar as many previous studies to carry out the CFD simulations, the models were input to ABAQUS 6.16 [41–43]. The temperature of exhaust gas from the car's engine is considered approximately 773–973 K [44]; after passing through the catalytic converter and several connecting pipes, the gas temperature drops to 623 K, due to local and frictional losses and heat leaks in the exhaust path. Therefore, the gas inlet temperature was considered as 600 K. The density, specific heat, viscosity, and thermal conductivity were taken to be 0.580 ρ (kg m^{-3}), 1.051 c_p (kJ kg^{-1} K^{-1}), 3.06 × 10^{-5} (Pa s), and 0.0466 k(W m^{-1} K^{-1}), respectively [16]. When the gas temperature reaches 573 K, the engine exhaust velocity reaches 15–20 m s^{-1} [18]. In all of the models, the fluid velocity at the inlet pressure and the outlet pressure were taken to be, respectively, 15.2 m s^{-1} and 0 Pa [21]. The no-slip boundary conditions were used for the external fluid boundary. It is worth mentioning that the output power of the TEG was computed using Eq. 8 according to the values in Table 1 [45, 46]:

$$P = \frac{\alpha^2}{2\rho}\frac{NA\Delta T^2}{(l+n)(1+2rl_c/l)} \tag{8}$$

where α and ρ are, respectively, the Seebeck coefficient and the electrical resistivity in thermocouple materials. N is the number of thermocouples in the module, A represents the cross-sectional area of the thermoelements, l_c is the thickness of the insulating ceramic layers, $n = \rho_c/\rho$, and $r = \lambda/\lambda_c$ where ρ_c and λ_c, respectively, denote the electrical contact resistivity and the thermal contact conductivity, l is the length of the semiconductor, and ΔT is the temperature difference between the cold and hot sources.

It must be noted that in Eq. 8, the temperature of the cold source is taken as 363 K which is based on the temperature of the engine water [45]. Also, the hot source temperature is the cross-sectional temperature of the effective areas of the heat exchanger, obtained from the CFD simulation of each model and substituted in Eq. 8.

To calculate the pressure drop in the heat exchanger, the difference in the inlet and outlet pressures of the heat exchanger was determined using Eq. 9 [31]:

$$P_{drop} = P_{in} - P_{out} \tag{9}$$

where P_{in} and P_{out} represent the inlet pressure and the outlet pressure of the heat exchanger, respectively. It is worth noting that the values of P_{in} and P_{out} have been obtained from the thermal-CFD simulation.

Table 1 Parameters of PN materials [45, 46]

Parameter	P type	N type
Seebeck coefficient/μV K^{-1}	215	−215
Electrical resistivity/Ω m	1.04 × 10^{-5}	1.04 × 10^{-5}
Thermal conductivity/W m^{-1}K^{-1}	1.5	2.5
Height/m	0.005	0.005
Sectional area/m^2	0.01 × 0.01	0.01 × 0.01

The tetrahedron element type was used for meshing all the heat exchanger models. Also, for the mesh convergence study, three mesh strategies were implemented for each model. As such, the numbers of elements for the coarse, medium, and fine meshing of models A were, respectively, 287,022, 332,119, and 335,583. The corresponding numbers were 366,408, 400,656, and 401,402 for models B and 50,221, 70,960, and 73,656 for models C. The results obtained from the grid independence study indicate that the difference in the maximum velocity results between the medium and fine meshes in models A, B, and C was 0.51%, 1.08%, and 0.98%, respectively (Fig. 2). Overall, the difference between these two mesh types was less than 1.1% for all models. Hence, the independence of the results from the meshing and time step conditions and the convergence of the results are suitably guaranteed.

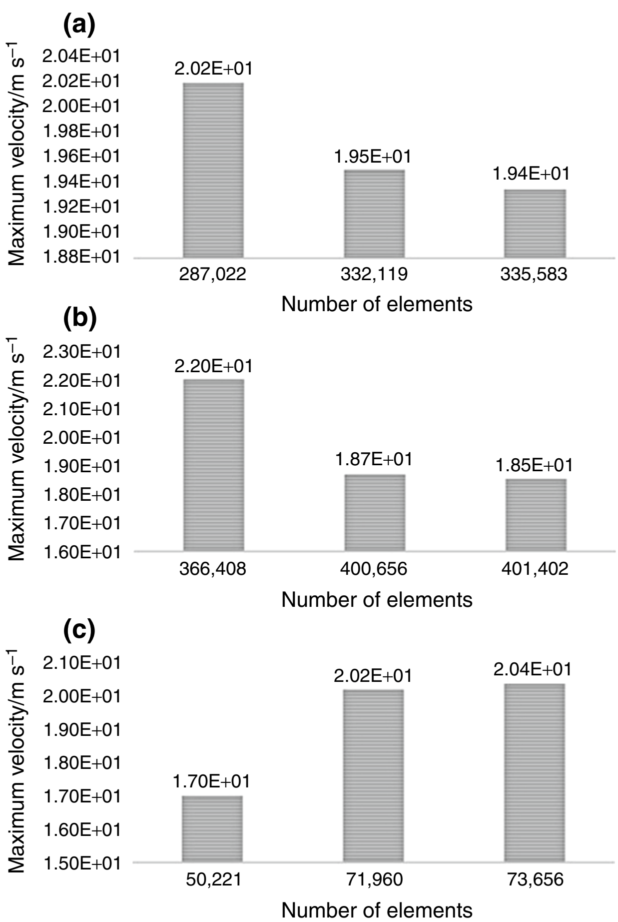

Fig. 2 Grid independence study results, **a**, **b**, and **c** comparison of maximum gas velocity for three meshing strategies: course, medium, and fine

Results and discussion

Data validation

Data validation is a major concern in computer simulations. To ensure the validity of the assumptions and the governing equations, it is necessary to measure the experimental results and compare them to the results calculated by the computer simulation. For this purpose, the maximum temperature in the heat exchanger was experimentally measured and compared to the simulation results. The experimental measuring of the maximum temperature confirmed according to previous researches [47, 48]. Figure 3 shows the experimental test procedure. The comparison results indicated that the maximum difference in the experimental and simulation values of temperature for this model was less than 3.2%. Thus, the validity of the computer simulation was confirmed. It must be noted that the experimental test of the other models was not feasible given the limitations of the research.

Temperature distribution in the heat exchanger with a different internal structure

To calculate the output power of the heat exchanger, it is required to calculate the temperature difference ΔT. For this purpose, the cold temperature was considered to be 363 K, according to the engine water temperature. However, the hot temperature was determined from the thermal-CFD simulation results according to the heat distributed to the top and

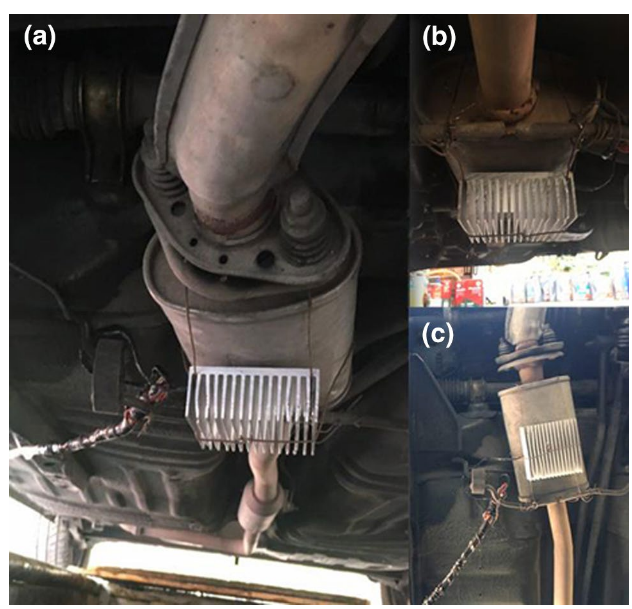

Fig. 3 Experimental thermal assessment of vehicle exhaust path, **a**, **b**, and **c** rear, front, and bottom views of the heat exchanger

bottom surfaces in the middle section of the model. The maximum temperature, which is a significant parameter in power assessment, was almost similar in all the models, as shown in Fig. 4. However, the baffle arrangement has only contributed to the optimal distribution of temperature to obtain a larger cross section with a higher temperature. It is observed in model A_1 that the placement of the baffles at the angle 50° in the front section, the 38.78 mm distance of the baffles from the inlet, and the 5 mm baffle thickness have together led to a more uniform and more optimal temperature distribution in the heat exchanger compared to the other models. This is because the average temperature of model A_1 is 2.81%, 16.87%, 5.09%, 4.39%, 14.58%, 9.49%, 8.08%, and 4.74% higher than those of models A_2, A_3, B_1, B_2, B_3, C_1, C_2, and C_3, respectively (Fig. 5a). Furthermore, the baffle arrangement in the middle section has caused the highest required temperature to be optimally distributed over a larger surface. However, in model A_2, the temperature distribution slightly tended toward the left side of the heat exchanger with a change in the baffle angle to 40° and an increase in the baffle distance from the inlet to 55.90 mm while keeping the same baffle thickness of 5 mm (Fig. 4). Moreover, in model A_3 which is similar to model A_1 with the only difference being its 10 mm baffle thickness, the maximum temperature value tended toward the right side of the heat exchanger (Fig. 4). Hence, it is concluded that the temperature has not distributed optimally and uniformly in the middle section of the heat exchanger in models A_2 and A_3. As a result, the access of the thermoelectric plate to the hot surface has been restricted. Subsequently, the baffle arrangement of model A_1 was repeated in model B_1 with a suitable angle and thickness for the baffles in the front section, while reducing the baffle height in the middle section to 2.30 mm. According to Fig. 4, the temperature distribution in a portion of the middle section is not uniform and optimal. Subsequently, a more optimal temperature distribution was attempted in model B_2 by increasing the distance between baffles in the middle section from 5.2 to 16.8 mm, which resulted in better temperature distribution over the surface of the heat exchanger. In model B_3, the front baffles were eliminated, and 2 deflectors were added to the middle section. As shown in Fig. 4, the temperature distribution is not uniform over the heat exchanger, and the maximum required temperature is in the middle section. In model C_1, the authors tried to prevent contact between the middle baffles and the top and bottom surfaces of the heat exchanger by neglecting the front baffles. This led to a 5.63% improvement in temperature distribution over the surface of the heat exchanger compared to model B_3 (Fig. 5a). As a result, the front baffles were again taken into account in model C_2, and unlike model A_1, the middle baffles were given a chaos-shaped arrangement. This, in turn, caused the temperature to tend to the left side of the heat exchanger while some portions of the middle section were not able to distribute optimally and uniformly over the heat exchanger surface. Finally, the baffle strategy was changed once again in model C_3. It is seen in Fig. 4 that the temperature is mostly tending to the right side; nevertheless, this model has a better temperature distribution than model C_2.

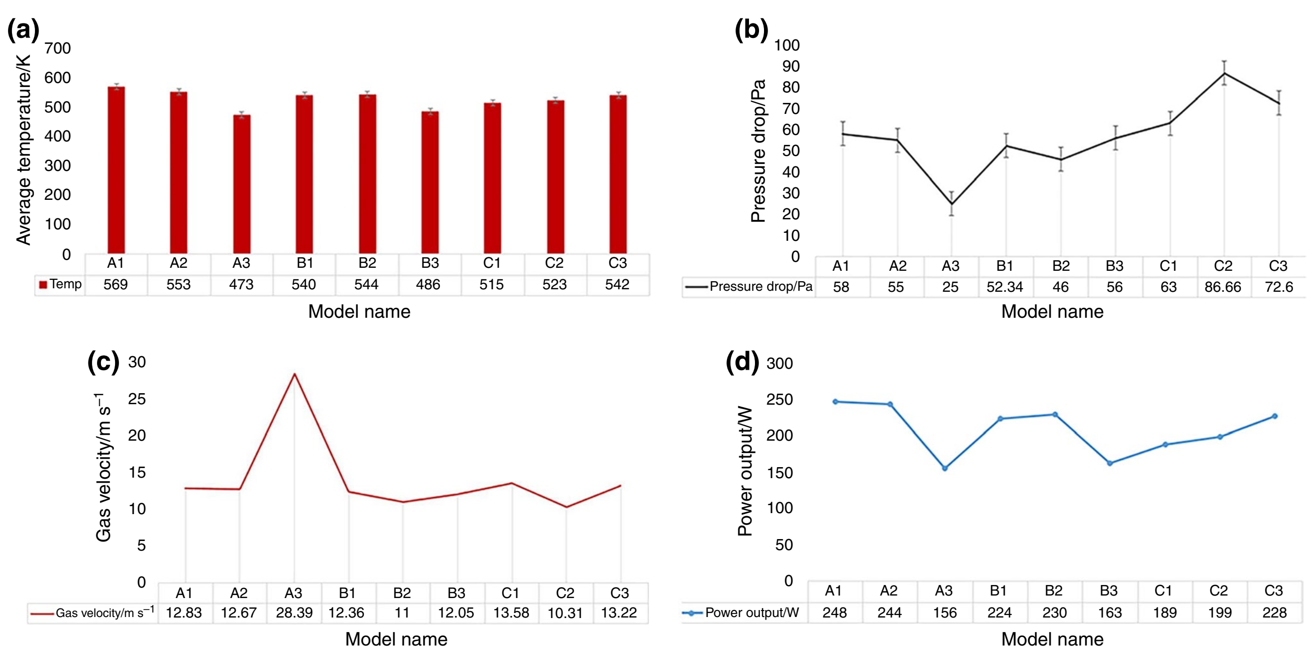

Fig. 4 **a** Graph showing the results average temperature over the middle surface of the heat exchanger, **b** graph of the pressure drop in the heat exchanger, **c** and **d** graphs of the maximum gas velocity in the heat exchanger and power generated by the thermoelectric modules

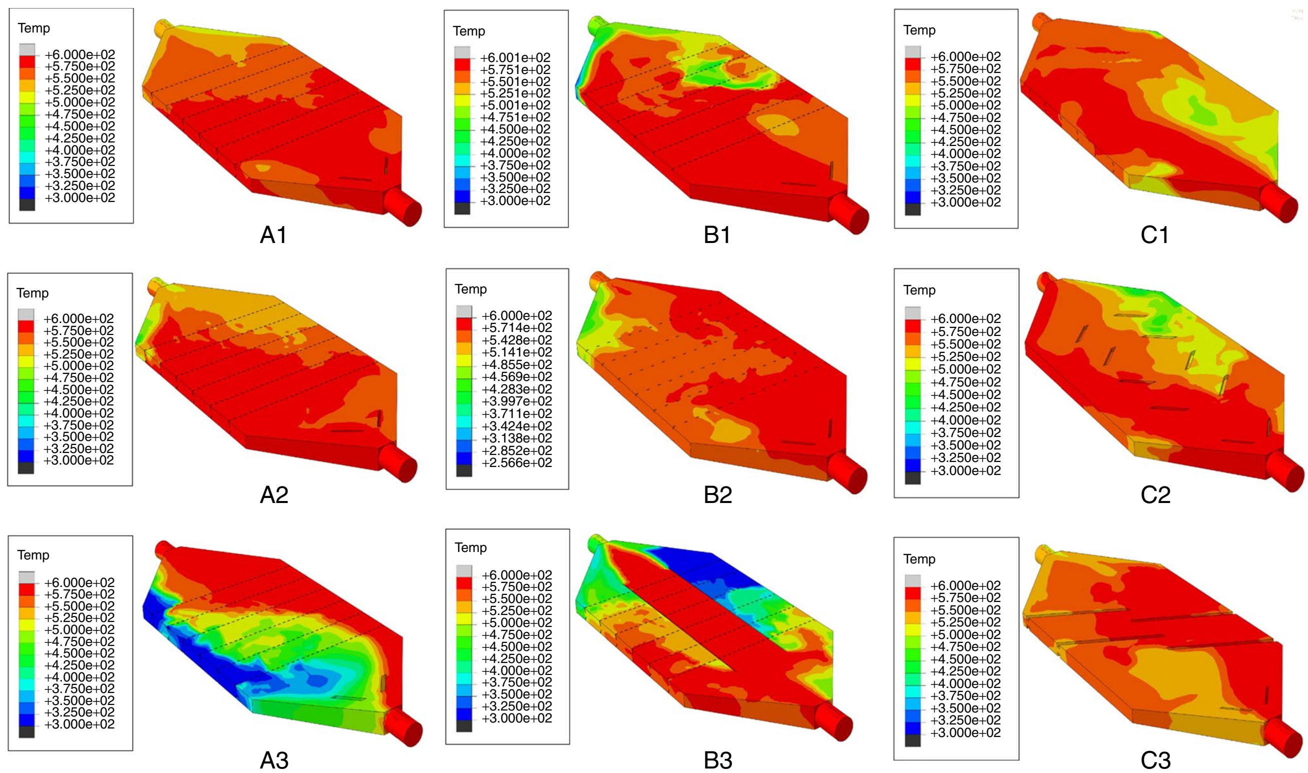

Fig. 5 Results of the temperature distribution over the surfaces of the nine heat exchangers with different internal structures

Based on the results of the CFD analyses of the 9 models, Fig. 5a shows that by applying a temperature of 600 K at the inlet of the heat exchanger, the average temperature on the desired surface in models A_1 and A_2 increased up to 569 K and 553 K, respectively. In the research by Deng et al. [18] which has almost model dimensions and an inlet similar to this research, the average temperature was reported to be 513 K. Consequently, the effectiveness of the baffle arrangement in models A_1 and A_2 in the present paper is, respectively, 9.84% and 7.23% higher than that of Deng et al. It must be noted that according to the research by Liu et al. the average temperature in the heat exchanger without fins or with the absence of an obstacle to temperature distribution was 373 K, increased to 520 K with the addition of small fins. This value was less than the corresponding values in models A_1 and A_2 by 8.61% and 5.96%, respectively [17].

An average temperature of 473 K was obtained in model A_3 due to an increase in the thickness of the front baffles, a change in the path of the required thermal flow, and the non-uniformity of the temperature distribution. This model is not suitable compared to models A_1 and A_2 because of the unidirectional distribution of temperature. The value of average temperature reached 540 K in model B_1 with a decrease in baffle height and increased only by 4 K in model B_2 with an increase in baffle distance in the middle section. Although these two models are better than model A_3, they have been less effective than models A_1 and A_2. It was observed in the results obtained from model B_3 that by adding 2 deflectors and eliminating the front baffles, one obtains an average temperature of 486 K, which is not an optimal temperature distribution. It is possible to use 2 baffles in the front section to optimize these conditions for achieving a uniform temperature distribution over the whole heat exchanger, similar to the research by Wang et al. [32]. In model C_1, which has no baffles in the front section, the temperature was distributed unidirectionally, and the average temperature was 515 K. Hence, it can be deduced that placing baffles at the front of a heat exchanger has a significant impact on the optimal temperature distribution over the whole surface. In contrast, placing the baffles in the middle of model C_1 resulted in a higher required average temperature on the surface. By putting the baffles in a chaos-shaped arrangement in the heat exchanger in models C_3 and C_2, the obtained average temperature increased to 523 K and 542 K, respectively. It can be deduced from the results that the different arrangements in models B_2 and C_2 have led to almost similar temperature distributions; however, none of these two models have resolved the issues of non-uniform temperature distribution and larger access to the hot surface for the thermoelectric module.

Evaluation of gas velocity and pressure

The velocity and pressure of the exhaust gas are according to the Bernoulli relationship. Increasing the gas velocity at the exhaust outlet is important; however, this increase leads to a decrease in pressure. The maximum permissible pressure drop in the exhaust system is 190 kPa, and in case the pressure drop exceeds this limit, it is necessary to use a bypass mechanism to ensure the stability and reliability of the engine [11]. As shown in Fig. 5b, the largest pressure drop and smallest pressure drop have occurred in models C_2 and A_3 with the values of 86.66 Pa and 25 Pa, respectively. In addition, the calculated pressure drop in model C_2 was higher than those in models A_1, A_2, A_3, B_1, B_2, B_3, C_1, and C_3 by 36.53%, 33.07%, 71.15%, 39.60%, 46.91%, 35.37%, 27.30%, and 19.15%, respectively. Moreover, the pressure drop in model C_3 is 70.06 Pa. The large pressure drop in models C_2 and C_3 may be related to the chaos-shaped baffle arrangement strategy. The gas velocity in regions with high temperature reaches 10.30 m s^{-1} in model C_1 and 13.22 m s^{-1} in model C_3 (Fig. 6). The baffle arrangement combined with the presence of front baffles in model C_3 has led the maximum gas velocity to the right side of the heat exchanger. Also, the baffle arrangement in the middle of model C_2 has led most of the high-velocity region to the left side of the heat exchanger. The elimination of the baffles in the front part of model C_1 has caused the gas velocity in the high-temperature regions to reach 13.58 m s^{-1} and the pressure drop in model C_1 to be less than those in models C_2 and C_3, reaching 63 Pa. The distribution of velocity streamlines is displayed in Fig. 6, indicating that the velocity is high in the beginning but reduces when the flow collides with the baffles in the first row. After the gas passes the middle section of the heat exchanger, its velocity increases in the rear section. However, according to the same figure, the presence of the deflector in model B_3 results in the maximum gas velocity to be in the middle section. In this section, the velocity reaches 12.05 m s^{-1}, and the pressure drop reaches 56 Pa. It is worth noting that the maximum gas velocity in model B_3 has occurred at the inlet and outlet sections of the heat exchanger, as shown in Fig. 6. In the research by Wang et al. [32], 1683 Pa of backpressure was created by adding baffles in the front section and placing 10 cylinder grooves beside the deflector to control the velocity and the pressure in all of the heat exchanger. In the present research, in addition to achieving a better average temperature, a pressure drop value better than that in the research by Wang et al. was obtained. The pressure drop in models B_1 and B_2 is, respectively, 52.34 Pa and 46 Pa, indicating that increasing the distance between baffles in the middle section has reduced the pressure drop in the heat exchanger. This difference in the distance has also caused the velocity in the high-temperature regions of model B_1 to reach 12.36 m s^{-1} and that in model B_2 to fall to 11 m s^{-1}. It must be noted that these conditions have resulted in the creation of vortex in the heat exchanger in the 2 models (Fig. 6). This phenomenon has somewhat disturbed the distribution of the velocity streamlines. As mentioned earlier, the increase in the baffle thickness to 10 mm in model A_3 has guided the temperature distribution to one side of the heat exchanger and has caused a non-uniform temperature of the optimal gas temperature. The pressure drop in this model was 25 Pa, and the velocity was 28.39 m s^{-1}, as shown in Fig. 4c. This high velocity and small pressure drop have led the gas to exit the heat exchanger rapidly and have a smaller temperature impact on the surface (Figs. 4 and 6). Moreover, model A_3 is not in good conditions in terms of temperature distribution and gas velocity despite having a very good pressure drop. The pressure drops in models A_1 and A_2 are close, measuring at 58 Pa and 55 Pa, respectively (Fig. 5b). In model A_1, the gas

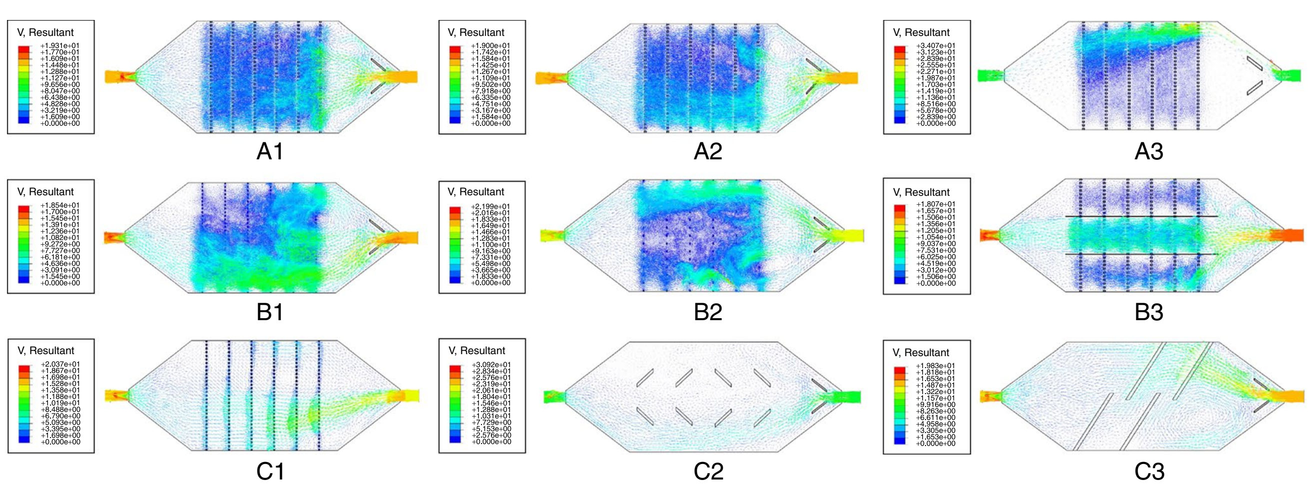

Fig. 6 Results of the distribution of gas velocity streamline in the nine different heat exchanger internal structures

velocity in high-temperature areas reaches 12.83 m s^{-1}, but in model A_2, it reduces to 12.67 m s^{-1} owing to the change in the baffle angle in the front section. According to Fig. 6, for both models, the velocity distribution is more optimal and uniform in the middle section of the heat exchanger, and the gas velocity increases in the rear section. It is worth mentioning that, according to the research by Niu et al [16], the number of baffles affects the pressure drop, and the pressure drop in this research increases up to 126.1 Pa. In the study by Su et al. [24], the pressure drop reaches 5000 Pa due to the difference in the folded plates in terms of length and thickness. In the paper by Liu et al., where the heat exchanger is between the catalytic converter and the muffler, given the many small fins inside the heat exchanger, the pressure drop was 127 Pa at an engine rotation rate of 3000 r min^{-1}, compared to the 9 models studied in the present research [22]. In the research by Liu et al., the pressure drop due to the many small fins reaches 210 Pa at an inlet pressure of 673 K. However, the results of the present research are better than previous research since the maximum pressure drop in the worst model is considerably lower than those in other research. Given the fact that the pressure drop was acceptable in all the nine models and although that model A_3 had the highest gas velocity, it is still not a good model overall due to its unacceptable temperature distribution. There were two main concerns for selecting the best choice among these models: one of them is the effect of the maximum of pressure drop and velocity, and the other is the distribution of temperature through the area. Therefore, models A_1 and A_2 are the best models since their pressure drop is in an acceptable range and their velocity had merely a slight difference from those of the other models.

Output power calculation

In this section, the efficiency of models will be compared based on the powers of models for finding the most effective arrangement of baffles. Considering the 60 thermoelectric modules with rectangular dimensions 390 mm by 310 mm on the top and bottom surfaces in the middle section, the output power of each thermoelectric module is calculated using Eq. 8, and total power of the 60 modules has been determined, as shown in Fig. 1b. The highest total output power belongs to models A_1 and A_2, with values of 248 W and 244 W, respectively (Fig. 5d). This is due to the optimal and uniform distribution and the high velocity of the required heat on the whole surface of the heat exchanger. The maximum power in the research by Liu et al. [21] in a rectangular heat exchanger with an area 4% less than that of the present paper was reported to be 183.24 W. The output power of models A_1 and A_2 was 26.11% higher than that in the research by Liu et al. In model A_3, the temperature distribution tended to one side with the increase in baffle thickness; hence, a smaller surface area of the heat exchanger had the temperature required for power generation in the TEG. As a result, the total output power has been 156 W in this model. By reducing the baffle height down to 2.30 mm in model B1 compared to model A_1, the output power in model B_1 is observed to reach 224 W (Fig. 5d). Also, creating a 16.8-mm distance between the baffles in model B_2 has caused the output power to be a little higher than that in B1 and the total output power of the TEG to reach 230 W. Thus, the increase in the distance between baffles in the middle section from 5.2 to 16.8 mm has led to only a slight increase of 2.60% in the output power. In models B_3, the presence of the deflector and the lack of uniform temperature distribution on the surface of the heat exchanger have caused the output power to be 163 W, 34.27% lower than that of A_1. On the other hand, by creating baffles in the front section of the heat exchanger, one can increase the output power up to 207.8 W, which is accompanied by an increase in pressure drop. The temperature distribution without baffles in the front section and merely guiding the gas flow in the middle section using baffles in model C_1 have led to the generation of 189 W of power. Also, using 8 baffles in the middle section in model C_2 resulted in 199 W of output power from the TEG. The baffle arrangement in model C_3 has caused 228 W of output power to be recorded, a better performance compared to model C_2. Therefore, similar to the results corresponding to the maximum and distribution temperature, pressure drop, and gas velocity, the power output obtained from the 9 models verifies that models A_1 and A_2 have led to higher power output, furthermore, the powers of models A_1 and A_2 are even better than in previous research.

Limitations and future works

Maintaining system security is a significant issue in TEGs. This is because the unit using the electric potential difference recovered by TEGs operates at a specific power and electric conditions, but the power generated by TEGs can vary based on engine rpm, combustion conditions, airflow, etc. In addition to vibration control [49], open-loop or closed-loop maximum power point tracking (MPPT) control systems were proposed [50], and Carstens et al. [51] have conducted numerous studies to eliminate the limitation of these systems in supporting a large number of TEGs. Hence, it is suggested that in future research, intelligent systems for controlling the ΔT generated by TEGs be presented to maintain the power resulting, according to new technology for solving heat equations [52], from the potential difference created by TEGs in the range required by the consumer. Furthermore, the effect of cold temperature is considerable for increasing the efficiency of the generators [53]. Hence, cold temperature control may be used for this purpose since the hot temperature can be different based on the conditions required by the vehicle user, and ΔT and power output can be kept in the desired range by controlling the cold temperature.

Conclusions

In this study, using thermal-CFD analyses, nine different heat exchanger models with various configurations were emulated and practically examined, and the electrical output power of the TEG for each case were studied.

The best configurations to obtain maximum power were introduced and evaluated via practical measurement. It was shown that the output power will experience its highest value in the models A_1 and A_2, and the lowest power will obtain via the model A_3 with the values of 248 W, 244 W, and 156 W respectively. Increasing the baffle thickness from 5 mm to 10 mm in the front section of the model A_3 supported the gas flow and prevented the temperature from distributing uniformly across the surface; however, less electrical power was produced, and the pressure dropped for 25 Pa. Also, the decrease in the baffle height from 8.46 mm to 2.30 mm in the middle section was studied through the model B1 and we obtained an average temperature of 5.09% lower than the model introduced in A_1 while the output electrical power was also decreased to 221 W.

Using a baffle height of 2.30 mm and increasing the distance between baffles from 5.2 mm to 16.8 mm in the model B_2, the distribution of the average temperature was increased by 0.73%, and the generated power was changed to 230 W. With the elimination of the front baffles in the models B_3 and C_1, it was observed that one cannot achieve an optimal temperature distribution over the heat exchanger surface by merely using deflectors and baffles in the middle section. The chaos-shaped baffle arrangement in models C_2 and C_3 resulted maximum pressure drops, for 86.66 Pa and 70.06 Pa respectively. However, it also led to power output values lower than the model A_1 by 19.75% and 8.06%, respectively.

Authors' contributions SG contributed to design of study; SG, RS, and MB were involved in the conceptualization; SG, RS, HF and MB contributed to methodology; SG, RS, MG, and MMT were involved in the formal analysis and investigation; RS was involved in writing—original draft preparation; RS, and MMT contributed to writing—review and editing; SG was involved in supervision. All authors approved the final manuscript.

Compliance with ethical standards

Conflict of interest The authors declare that they have no conflict of interest.

References

1. Sarafraz MM, Safaei MR, Tian Z, Goodarzi M, Bandarra Filho EP, Arjomandi M. Thermal assessment of nano-particulate graphene-water/ethylene glycol (WEG 60: 40) nano-suspension in a compact heat exchanger. Energies. 2019;12(10):1929.
2. Sarafraz MM, Safaei MR, Goodarzi M, Yang B, Arjomandi M. Heat transfer analysis of Ga-In-Sn in a compact heat exchanger equipped with straight micro-passages. Int J Heat Mass Transf. 2019;1(139):675–84.
3. Hosseini SM, Safaei MR, Estellé P, Jafarnia SH. Heat transfer of water-based carbon nanotube nanofluids in the shell and tube cooling heat exchangers of the gasoline product of the residue fluid catalytic cracking unit. J Therm Anal Calorim. 2019;21:1–2.
4. Sadeghinezhad E, Kazi SN, Sadeghinejad F, Badarudin A, Mehrali M, Sadri R, Safaei MR. A comprehensive literature review of bio-fuel performance in internal combustion engine and relevant costs involvement. Renew Sustain Energy Rev. 2014;1(30):29–44.
5. Wu C. Analysis of waste-heat thermoelectric power generators. Appl Therm Eng. 1996;16(1):63–9.
6. Hatzikraniotis E, Zorbas KT, Samaras I, Kyratsi TH, Paraskevopoulos KM. Efficiency study of a commercial thermoelectric power generator (TEG) under thermal cycling. J Electron Mater. 2010;39(9):2112–6.
7. LeBlanc S. Thermoelectric generators: linking material properties and systems engineering for waste heat recovery applications. Sustain Mater Technol. 2014;1(1):26–35.
8. Chen L, Gong J, Sun F, Wu C. Effect of heat transfer on the performance of thermoelectric generators. Int J Therm Sci. 2002;41(1):95–9.
9. Thacher EF, Helenbrook BT, Karri MA, Richter CJ. Testing of an automobile exhaust thermoelectric generator in a light truck. Proc Inst Mech Eng Part D J Autom Eng. 2007;221(1):95–107.
10. Kumar RC, Sonthalia A, Goel R. Experimental study on waste heat recovery from an IC engine using thermoelectric technology. Therm Sci. 2011;15(4):1011–22.
11. Bai S, Lu H, Wu T, Yin X, Shi X, Chen L. Numerical and experimental analysis for exhaust heat exchangers in automobile thermoelectric generators. Case Stud Therm Eng. 2014;1(4):99–112.
12. Saidur R, Rezaei M, Muzammil WK, Hassan MH, Paria S, Hasanuzzaman M. Technologies to recover exhaust heat from internal combustion engines. Renew Sustain Energy Rev. 2012;16(8):5649–59.
13. Love ND, Szybist JP, Sluder CS. Effect of heat exchanger material and fouling on thermoelectric exhaust heat recovery. Appl Energy. 2012;89(1):322–8.
14. Lu C, Wang S, Chen C, Li Y. Effects of heat enhancement for exhaust heat exchanger on the performance of thermoelectric generator. Appl Therm Eng. 2015;5(89):270–9.
15. Esarte J, Min G, Rowe DM. Modelling heat exchangers for thermoelectric generators. J Power Sources. 2001;93(1–2):72–6.
16. Niu Z, Diao H, Yu S, Jiao K, Du Q, Shu G. Investigation and design optimization of exhaust-based thermoelectric generator system for internal combustion engine. Energy Convers Manag. 2014;1(85):85–101.
17. Liu X, Yu CG, Chen S, Wang YP, Su CQ. Experiments and simulations on a heat exchanger of an automotive exhaust thermoelectric generation system under coupling conditions. J Electron Mater. 2014;43(6):2218–23.
18. Deng YD, Liu X, Chen S, Tong NQ. Thermal optimization of the heat exchanger in an automotive exhaust-based thermoelectric generator. J Electron Mater. 2013;42(7):1634–40.
19. Su CQ, Wang WS, Liu X, Deng YD. Simulation and experimental study on thermal optimization of the heat exchanger for

automotive exhaust-based thermoelectric generators. Case Stud Therm Eng. 2014;1(4):85–91.
20. Su CQ, Zhu DC, Deng YD, Wang YP, Liu X. Effect of cooling units on the performance of an automotive exhaust-based thermoelectric generator. J Electron Mater. 2017;46(5):2822–31.
21. Liu X, Deng YD, Zhang K, Xu M, Xu Y, Su CQ. Experiments and simulations on heat exchangers in thermoelectric generator for automotive application. Appl Therm Eng. 2014;71(1):364–70.
22. Liu X, Deng YD, Chen S, Wang WS, Xu Y, Su CQ. A case study on compatibility of automotive exhaust thermoelectric generation system, catalytic converter and muffler. Case Stud Therm Eng. 2014;1(2):62–6.
23. Wang Y, Wu C, Tang Z, Yang X, Deng Y, Su C. Optimization of fin distribution to improve the temperature uniformity of a heat exchanger in a thermoelectric generator. J Electron Mater. 2015;44(6):1724–32.
24. Su CQ, Huang C, Deng YD, Wang YP, Chu PQ, Zheng SJ. Simulation and optimization of the heat exchanger for automotive exhaust-based thermoelectric generators. J Electron Mater. 2016;45(3):1464–72.
25. Hatami M, Ganji DD, Gorji-Bandpy M. CFD simulation and optimization of ICEs exhaust heat recovery using different coolants and fin dimensions in heat exchanger. Neural Comput Appl. 2014;25(7–8):2079–90.
26. Fernández-Yañez P, Armas O, Capetillo A, Martínez-Martínez S. Thermal analysis of a thermoelectric generator for light-duty diesel engines. Appl Energy. 2018;15(226):690–702.
27. Golparvar B, Niazmand H, Sharafian A, Hosseini AA. Optimum fin spacing of finned tube adsorber bed heat exchangers in an exhaust gas-driven adsorption cooling system. Appl Energy. 2018;15(232):504–16.
28. Shu G, Ma X, Tian H, Yang H, Chen T, Li X. Configuration optimization of the segmented modules in an exhaust-based thermoelectric generator for engine waste heat recovery. Energy. 2018;1(160):612–24.
29. Su CQ, Ye BQ, Guo X, Hui P. Acoustic optimization of automotive exhaust heat thermoelectric generator. J Electron Mater. 2012;41(6):1686–92.
30. Wang Y, Li S, Yang X, Deng Y, Su C. Numerical and experimental investigation for heat transfer enhancement by dimpled surface heat exchanger in thermoelectric generator. J Electron Mater. 2016;45(3):1792–802.
31. Li S, Wang Y, Wang T, Yang X, Deng Y, Su C. Optimization of heat exchangers with dimpled surfaces to improve the performance in thermoelectric generators using a Kriging model. J Electron Mater. 2017;46(5):3062–70.
32. Wang Y, Li S, Zhang Y, Yang X, Deng Y, Su C. The influence of inner topology of exhaust heat exchanger and thermoelectric module distribution on the performance of automotive thermoelectric generator. Energy Convers Manag. 2016;15(126):266–77.
33. Zhu DC, Su CQ, Deng YD, Wang YP, Liu X. The influence of the inner topology of cooling units on the performance of automotive exhaust-based thermoelectric generators. J Electron Mater. 2018;47(6):3320–9.
34. Lu X, Yu X, Qu Z, Wang Q, Ma T. Experimental investigation on thermoelectric generator with non-uniform hot-side heat exchanger for waste heat recovery. Energy Convers Manag. 2017;15(150):403–14.
35. Wang Y, Li S, Xie X, Deng Y, Liu X, Su C. Performance evaluation of an automotive thermoelectric generator with inserted fins or dimpled-surface hot heat exchanger. Appl Energy. 2018;15(218):391–401.
36. Feng GA, Xiao-Jun YA, Zhang YF. Exact traveling wave solutions for a new non-linear heat transfer equation. Therm Sci. 2017;1(21):1833–8.
37. Yang XJ, Yang X, Zhu M. A new technique for solving the 1-D Burgers equation. Therm Sci. 2017;1(21):129–36.
38. Gholampour S, Jalali A. Thermal analysis of the dentine tubule under hot and cold stimuli using fluid–structure interaction simulation. Biomech Model Mechanobiol. 2018;17(6):1599–610.
39. Gholampour S, Hajirayat K. Minimizing thermal damage to vascular nerves while drilling of calcified plaque. BMC Res Notes. 2019;12(1):338.
40. Taher M, Gholampour S. Effect of ambient temperature changes on blood flow in anterior cerebral artery of patients with skull prosthesis. World Neurosurg. 2020 (**In press**).
41. Gholampour S. FSI simulation of CSF hydrodynamic changes in a large population of non-communicating hydrocephalus patients during treatment process with regard to their clinical symptoms. PLoS ONE. 2018;13(4):e0196216.
42. Gholampour S, Taher M. Relationship of morphologic changes in the brain and spinal cord and disease symptoms with cerebrospinal fluid hydrodynamic changes in patients with Chiari malformation type I. World Neurosurg. 2018;1(116):e830–9.
43. Gholampour S, Gholampour H, Khanmohammadi H. Finite element analysis of occlusal splint therapy in patients with bruxism. BMC Oral Health. 2019;19(1):205.
44. Braess HH, Seiffer U. Handbook of automotive engineering (English version). Warrendale: SAE International; 2005.
45. Min G, Rowe DM. Recent concepts in thermoelectric power generation. In: Twenty-first international conference on thermoelectrics. Proceedings ICT'02. IEEE; 2002. pp 365–74.
46. Liu X, Li C, Deng YD, Su CQ. An energy-harvesting system using thermoelectric power generation for automotive application. Int J Electr Power Energy Syst. 2015;1(67):510–6.
47. Gholampour S, Deh HH. The effect of spatial distances between holes and time delays between bone drillings based on examination of heat accumulation and risk of bone thermal necrosis. Biomed Eng Online. 2019;18(1):65.
48. Gholampour S, Shakouri E, Deh HH. Effect of drilling direction and depth on thermal necrosis during tibia drilling: an in vitro study. Technol Health Care. 2018;26:687–97.
49. Mahdisoozani H, Mohsenizadeh M, Bahiraei M, Kasaeian A, Daneshvar A, Goodarzi M, Safaei MR. Performance enhancement of internal combustion engines through vibration control: state of the art and challenges. Appl Sci. 2019;9(3):406.
50. De Brito MA, Galotto L, Sampaio LP, e Melo GD, Canesin CA. Evaluation of the main MPPT techniques for photovoltaic applications. IEEE Trans Ind Electr. 2013;60(3):1156–67.
51. Carstens JH, Gühmann C. Maximum power point controller for thermoelectric generators to support a vehicle power supply. Mater Today Proc. 2015;2(2):790–803.
52. Yang XJ, Gao F. A new technology for solving diffusion and heat equations. Therm Sci. 2017;21(1A):133–40.
53. Bahiraei M, Salmi HK, Safaei MR. Effect of employing a new biological nanofluid containing functionalized graphene nanoplatelets on thermal and hydraulic characteristics of a spiral heat exchanger. Energy Convers Manag. 2019;15(180):72–82.

Publisher's Note Springer Nature remains neutral with regard to jurisdictional claims in published maps and institutional affiliations.